This is a preprint of the following article, which is available at: http://mdolab.engin.umich.edu
Marco Mangano and J. R. R. A. Martins. Multipoint Aerodynamic Shape Optimization for Subsonic and Supersonic Regimes. *Journal of Aircraft*, In press, July 2020.
The original article may differ from this preprint and is available at:
https://doi.org/10.2514/1.C036216.

Multipoint Aerodynamic Shape Optimization for Subsonic and Supersonic Regimes

Marco Mangano and Joaquim R. R. A. Martins
University of Michigan, Ann Arbor, MI, 48109

Abstract

The second-generation of supersonic civil transport has to match ambitious targets in terms of efficiency to be economically and environmentally viable. CFD-based design optimization offers a powerful approach to address the complex tradeoffs intrinsic to this novel configuration. We apply this approach to the design of airfoils and wings at both supersonic cruise conditions and lower-speed, off-design conditions. We perform single and multipoint optimization to minimize the drag over an ideal supersonic aircraft flight envelope and assess the influence of physical and numerical parameters on optimization accuracy and robustness. To obtain more favorable design tradeoffs between different flight regimes, we introduce morphing leading and trailing edge capabilities, and quantify their benefits against fixed-wing shapes. The optimized layouts outperform baseline supersonic reference designs over a range of flight conditions, with drag reductions from 4% up to 86% for airfoils, and between 24% and 74% reductions relative to a reference wing. The results demonstrate that the proposed approach enables the fast and effective design of highly-efficient wings, capturing non-intuitive tradeoffs, and offering more in-depth physical insight into the optimal layouts.

1 Introduction

After the first supersonic flight by Chuck Yeager on October 14, 1947, supersonic aircraft technology has made enormous leaps in some areas, but has fallen short in others. While flying faster than sound has become routine for military aircraft, there is currently no supersonic transport (SST) aircraft in service. Technological limitations and related economic issues have prevented the establishment of a new generation of supersonic aircraft since the decommissioning of the Concorde in 2003 [1]. Sonic-boom reduction and flight efficiency improvement are cited as significant issues in the design of the next generation of SST. Reducing supersonic cruise fuel burn is an intricate design problem that needs to be addressed, while taking into account

the impact of off-design, low-speed flight segments on the overall fuel consumption. Furthermore, current regulations forbid supersonic flight overland due to the damage and discomfort caused by sonic-booms at ground level. This implies that novel designs have to consider both noise reduction strategies and aerodynamic tradeoffs to reduce the drag penalty when flying at transonic regimes over populated areas, which is more realistic in the short term. On the one hand, innovative technologies focused on boom signature reduction * [2] and drag minimization using natural laminar flow (NLF) technology [3–5] have shown promising results . On the other hand, multidisciplinary design optimization (MDO) and aerodynamic shape optimization (ASO) [6] techniques offer a powerful approach to design an efficient supersonic aircraft [7]. Unlike other conventional and unconventional subsonic transports, supersonic aircraft configurations have not been thoroughly investigated using design optimization in recent years.

Since the 1970s, early ASO studies investigated supersonic airfoil design [8], highlighting how theory from Von Karman [9], Munk [10], and Tsien and Baron [11] could not predict more complex compressibility and viscosity effects, even for simplified cases. As the computational capabilities evolved, Reuther et al. [12], Reuther and Jameson [13], Reuther et al. [14] and Kim et al. [15] used an Euler solver with an adjoint-method approach to improve aerodynamic performance [16]. The advantages of simultaneous multipoint optimization over single-point sequential strategies were at this stage already acknowledged [17]. More extensive gradient-based ASO and MDO studies for conceptual and mission design further highlighted the computational-cost limitations of CFD-based tools, together with an overall weakness of the frameworks in terms of geometry and mesh manipulation capabilities. These software limitations affected several promising works focused on multidisciplinary and multipoint optimization [18–22] and mission optimization [23–25]. The use of inviscid CFD solvers was limited to cruise conditions, with viscous effects and off-design performance obtained via analytical and semi-empirical approaches. The additional implementation effort to obtain coupled disciplines sensitivities was often avoided by using less efficient gradient-free approaches. Jameson et al. [26] successfully used a continuous adjoint approach but were limited by their flow solver and parametrization scheme, while Choi et al. [27] obtained partial improvements by including a low-fidelity response-surface model in their framework.

Alternative strategies based on surrogate modeling and genetic optimization algorithms explore the design space more extensively [28–30], although with a higher computational cost and lower-accuracy aerodynamic models [31]. Comparative studies underline the higher efficiency of the gradient-based strategies even for SST design, although overly stressing the potential shortcomings due to the possible presence of local minima [32].

Martins et al. [33] performed the aerostructural optimization of a supersonic business jet (SSBJ) by successfully implementing coupled aerodynamic and structural adjoint equations to calculate sensitivities. They showed how the computational cost is nearly independent from the number of design variables with this optimization strategy. Even if noise signature considerations are out of the scope of this work, it is worth

*Quiet Supersonic X-plane: https://www.lockheedmartin.com/en-us/products/quesst.html

mentioning that the adjoint method has been successfully applied to sonic-boom reduction studies [34–36], further demonstrating the potential of gradient-based optimization applied to SST configurations.

More recent studies on SST design optimization focused on broader framework implementation, including multifidelity and model uncertainty [37], more efficient integration of aircraft design sub-disciplines [38–40], and combining preliminary aircraft sizing with aerodynamic analysis [41, 42]. While these efforts underline the high interest in the topic and highlight the progress in computational efficiency and framework complexity, there is still a lack of emphasis on aerodynamic analysis accuracy and framework robustness for CFD-based design optimization.

In 2D aerodynamic shape optimization, few relevant efforts tackled the topic, as airfoil ASO has been generally included in the broader wing design. The Busemann biplane has been used as a test case for inviscid gradient-based ASO [43] and uncertainty quantification [44], while Kiyici and Aradag [41] obtained a diamond-shape section from a conventional NACA 6-digit airfoil. However, Lattarulo et al. [45] highlighted the offset between Euler-based and RANS-based analysis, highlighting the need to perform supersonic ASO considering viscous phenomena, even for 2D optimization.

Unconventional design solutions for drag reduction have not been thoroughly investigated with modern high-fidelity tools. Multiple patents [46–48] suggest that the implementation of slot-less and gap-less high-lift devices on supersonic aircraft wings is beneficial for low-speed performance. Varying wing camber can relax the aerodynamic tradeoff between subsonic and supersonic performance of the fixed airfoil shape, with limited mechanical complexity compared to variable-sweep wing configurations. Additionally, the detrimental effects due to the center-of-pressure shift between flight regimes can be minimized, reducing trim drag and aeroelastic couplings on thin-section wings. Early work suggested that transonic L/D could be improved by 10–20% [20, 21, 49], although these analyses did not take into account viscous effects. More relevant and accurate results could be obtained through RANS-based ASO.

No publicly available work focuses on RANS-based aerodynamic optimization of SST design concepts with state-of-the-art tools and considers both the 2D wing section and the full wing design, also including multipoint strategies and edge deflections. In this paper, we aim to fill this gap by thoroughly investigating the drag minimization problem for lifting surfaces of an SST, and gain insight on both the physics and the numerical modeling influence on optimal design. Noise signature reduction, although relevant, is outside the scope of this paper.

The studies in this paper are carried out using the framework for MDO of aircraft configurations with high fidelity (MACH) [50], which can efficiently perform RANS-based ASO. The advantages of using a viscous solver for subsonic and transonic ASO problems have been highlighted in previous work [50–52], and include higher accuracy and more robust optimal designs. With our tool, we overcame modeling limitations and computational cost concerns that have prevented the extensive application of this methodology.

We initially assess the influence of different flight conditions and shape variable distributions on the optimal supersonic airfoil shape. The design space convexity is investigated by comparing multiple design cases starting from different initial geometries.

The optimization is then extended to include transonic and subsonic flight segments. The airfoil is optimized to minimize the average drag for a given speed versus altitude stencil, which is defined to match a reference transatlantic flight path. The drag reductions owing to gap-less leading and trailing edge deflections at off-design conditions are quantified and compared to a fixed-shape 2D optimization. We define a set of constraints to ensure that the optimal solution satisfies volume (or cross-sectional area), thickness, lift, and trim requirements. Following that, we extend the same methodology to a planar wing modeled on the Aerion AS2 [†] prototype planform. We include a set of spanwise deformation variables to allow the optimizer to manipulate the wing twist, together with an additional constraint on bending moment to maintain the structural feasibility of the final layout. These studies contribute to new insights into how physical and numerical parameters influence the airfoil and wing optimization accuracy and robustness, while also offering a benchmark for future work.

In Sec. 2, we present the tools used for this study, and in Sec. 3, we summarize the details of the optimization problem. Results for both 2D and 3D case studies are presented and discussed in Sec. 4 and summarized in Sec. 5.

2 Methodology

For the ASO studies in this work, we use the in-house developed and publicly-available MACH-Aero toolbox. [‡] The framework consists of a RANS-based CFD solver to model the flow coupled with an adjoint solver that efficiently computes shape sensitivities, a robust geometry and mesh perturbation algorithm, and a gradient-based optimizer. This ASO toolbox has been demonstrated to improve the aerodynamic performance of both conventional [53–55] and unconventional aircraft configurations [56–58].

The MACH-Aero geometry module, pyGeo, uses the free-form deformation (FFD) parametrization approach [59]. The implementation of this strategy to perform shape modifications in MACH is detailed by Kenway et al. [60]. A limited number of variables is used to control the deformation of a "flexible" control box that embeds the baseline geometry. This approach is compact and efficient because it does not parametrize the shape itself but rather its deformation, facilitating geometry sensitivity calculations. The assumption of fixed topology does not constrain the design space of the outer mold line of a single-element airfoil or even a wing.

A mesh perturbation scheme, IDwarp, propagates the surface deformations to the volume grid at each design iteration with an inexact explicit interpolation algorithm based on inverse distance weighting method [61]. A high-quality grid is thus guaranteed even for large deformations, at the cost of 0.1% of a CFD solution [62]. Reverse-mode automatic differentiation is applied to calculate the volume node sensitivities with respect to the surface deformation.

The RANS aerodynamic analysis and sensitivity calculation via the adjoint method in this work is performed by ADflow [63–65]. We select the Spalart–Allmaras [66] turbulence model for this optimization study.

[†]Aerion Supersonic Website: https://www.aerionsupersonic.com

[‡]https://github.com/mdolab/MACH-Aero

To efficiently search the design space, we choose the gradient-based optimizer, SNOPT [67]. This is connected to the MACH framework using the pyOptSparse interface [68]. [§]

Yu et al. [69], as well as Chernukhin and Zingg [70], suggested that the 2D problem is unimodal for subsonic and transonic regimes, thus obviating the need for a global optimizer. They also showed that the gradient-based approach is more efficient than gradient-free algorithms when performing CFD-based airfoil optimization. It is reasonable to expect a convex design space for supersonic conditions as well, especially if viscous effects are taken into account [52]. As for the higher-dimensional design space for wing optimization, the gains in algorithm efficiency largely outweigh the risks of encountering a local minima [53, 71]. This assumption is reinforced by benchmarking the convergence of the different optimization cases with multiple baseline geometries.

3 Problem Formulation

In this section, we discuss our approach to the optimization problem in terms of formulation, modeling, and more practical tips. We introduce the baseline geometries to optimize, emphasizing the meshing details, and other expedients to improve the optimization robustness. Design variables for both the 2D and 3D problems are illustrated, together with the implementation and modeling of the morphing capabilities. Finally, we summarize the selection criteria for the flight conditions, geometric constraints, and performance constraints. Mangano and Martins [72] provides details on mesh quality and flow solver accuracy that are not included in the present paper.

3.1 Baseline Geometry

In contrast to constructive schemes, such as CST or B-splines, the FFD parametrization approach implies a potential influence of the initial geometry on the final shape [73]. To investigate this issue, we run our 2D optimization cases starting from multiple initial wing sections. Reference geometries are based on NACA 4-digit and 6-digit airfoil families, together with conventional transonic airfoils such as RAE 2822. A family of biconvex supersonic airfoils is generated using the NACA notation [74].

The presence of sharp leading edges on the typical supersonic airfoil poses a challenge for the geometry manipulation module. The control-point displacements can sharpen a smooth round shape, but the reverse process is not guaranteed as the initial surface is not C^2 continuous. For this reason, all the biconvex airfoils in this study present a small round edge to replace the ideally sharp leading edges, as shown in Fig. 1(a).

Given the initial geometry, the user-defined surface meshes with an appropriate chordwise point distribution are passed to pyHyp, a 3D hyperbolic grid generation scheme based on work by Chan and Steger [75]. [¶] We chose an O-grid topology due to its reduced computational cost and superior deformation robustness compared to

[§] https://github.com/mdolab/pyoptsparse

[¶] https://github.com/mdolab/pyhyp

C-grids. The grids used in this paper have undergone grid refinement studies to ensure a minimum discretization error at all the different flight conditions we introduce later in this section. The selected baseline wing geometry is shown in Fig. 1(b).

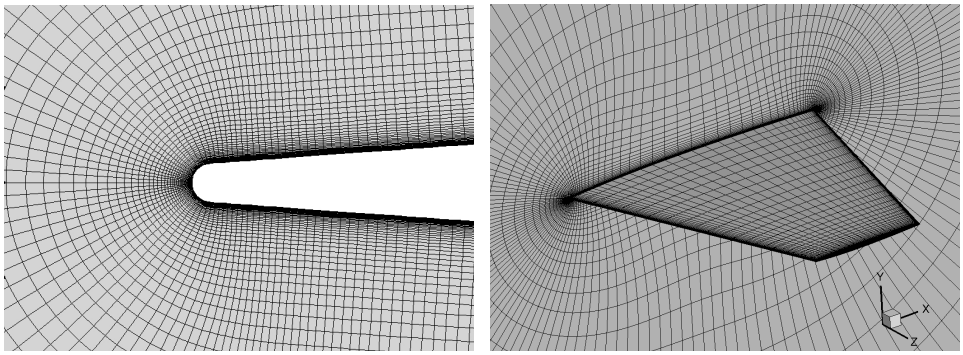

(a) (b)

Figure 1: (a) Detail of the rounded leading edge of a biconvex NACA 2S-(40)(1.5)-(40)(1.5) airfoil [74] and (b) the selected baseline wing mesh (750K elements).

For the baseline wing, we define a relatively simple trapezoidal planform using as reference the currently (October 2019) available information on the Aerion AS2 [‖]. We select the same NACA 2S-(40)(1.5)-(40)(1.5) airfoil from the 2D case study for the wing section. The geometry parameters are listed in Table 1.

Semi span	9.67[m]
Semi area	71.48[m^2]
Aspect ratio	2.6
Root chord	10.38[m]
Tip chord	4.4[m]
LE sweep	19.7[°]

Table 1: Baseline wing geometry data

3.2 Design variables

The optimizer has direct control on the local geometry manipulation. The airfoil is embedded in a $n \times 2 \times 2$ (chordwise, vertical and spanwise direction respectively) FFD grid, while the wing is parametrized by a $m \times 2 \times 4$, with equally spaced spanwise stations. n and m are arbitrary chosen numbers, selected to maximize the geometry deformation capabilities.

Control points only move along the vertical direction. For airfoil optimization, spanwise symmetry is imposed to avoid non-uniform spanwise deformations. The opti-

[‖]In May 2020 a new configuration for AS2 has been unveiled [76]. The details of the new design are discussed by Bons et al. [77]

mizer also controls the angle of attack (α) to match the different C_l constraints without excessive baseline geometry distortions.

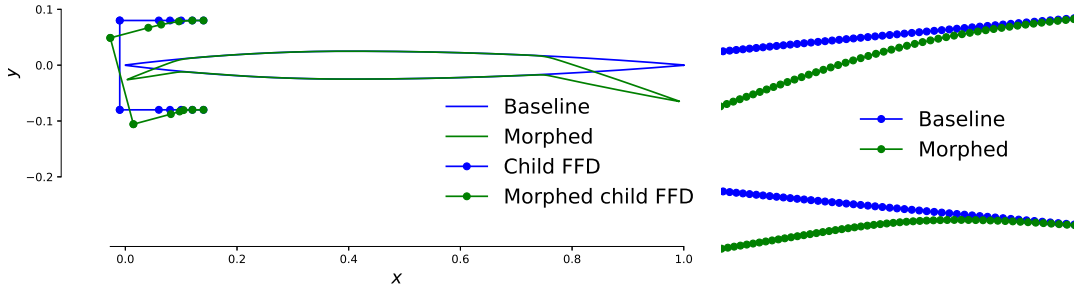

(a) Morphing airfoil parametrization (b) Virtual hinge detail

Figure 2: Example of the morphing leading and trailing edges for NACA 2S-(40)(015)-(40)(015) (a) and a detail of hinge deformation (b) for β_{LE}=−15°, β_{TE}=15°

The introduction of the morphing capabilities adds two geometric variables to the problem, namely the two deflection angles β_{LE} and β_{TE}, which vary independently for each flight condition. Two child FFD frames are attached to the main FFD to model these deflections. These child FFDs are allowed to rotate around a fixed virtual hinge, as schematically illustrated in Fig. 2(a). For both the airfoil and the wing, the virtual hinge locations are fixed at 10% and 75% of the chord for the leading and trailing edge, respectively. The rigid rotation of these sub-grids drives the deflections, while the local shape perturbation and wing twist remain under control of the main FFD variables. The distribution of the control points around the virtual hinge is arranged to limit the propagation of shape deformations along the airfoil surface [78], as highlighted in Fig. 2(b).

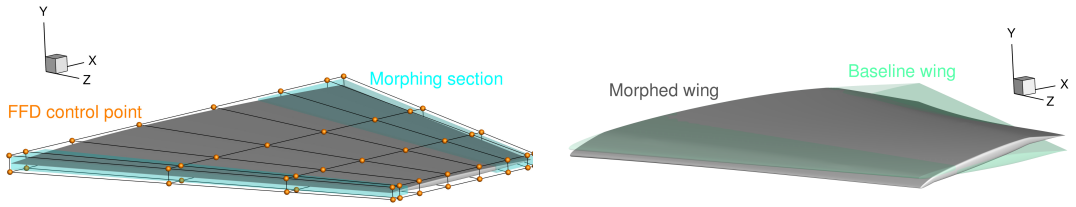

(a) Wing parametrization box (b) Wing manipulation test

Figure 3: Wing parametrization (a), and example deformed wing (b) with β_{LE}=−10°, β_{TE}=10° and $\text{twist}_{\text{tip}\rightarrow\text{inboard}}$ = [−10°, −5°,0°].

For the wing optimization cases, we extend the airfoil parametrization case to multiple, independent, and linearly-spaced spanwise stations. We add a global variable for the twist at each of these stations, excluding the root section, allowing a rigid rotation of the local control points around a virtual hinge located at 25% of the chord.

A snapshot of the complete parametrization grid around the baseline wing and an exemplifying wing deformation test are illustrated in Fig. 3.

3.3 Optimization Problem Formulation

Our objective is to minimize the drag of airfoils and wings for the supersonic cruise condition while taking into account low-speed, off-design performance. We gain insight into the design space characteristics and the influence of different physical and numerical parameters by exploring multiple optimization problems.

We use historical data [7, 79] **, and predicted performance of the Aerion AS2 to establish a realistic flight envelope for a SBBJ. We identify four different flight conditions, defined by Mach number, altitude, and lift coefficient: a supersonic cruise condition at high altitude ($M = 1.45$), a high transonic condition ($M = 1.15$, theoretically suitable for "boomless cruise"), a "conventional" transonic condition ($M = 0.95$), and a subsonic descent condition ($M = 0.44$ at 14,000 ft, to comply with FAA regulations on holding speed and altitude). Lift coefficients are estimated based on the Aerion AS2 predicted MTOW and wing area, considering a full fuel load for cruise cases and an approximately 15% fuel reserve for low-speed holding. For an ideal flight path from Paris to New York (CDG-JFK), we estimate an 85% of the route at unrestricted speed, 10% overland (thus at $M \leqslant 1.15$) and 5% at subsonic speed. The reference flight conditions we use are reported in Table 2, while the optimization problem is summarized in Table 3.

Case name	Mach	C_L	C_l	Altitude [m]([ft])
Supersonic	1.45	0.195	0.236	13,700 (45,000)
High transonic	1.15	0.2	0.3	11,000 (33,000)
Transonic	0.95	0.295	0.4	11,000 (33,000)
Subsonic	0.44	0.324	0.62	4,280 (14,000)

Table 2: Summary of the flight conditions for our optimization problems.

Design Variable	Qty	Constraints	Qty
Shape	24/32 for airfoil 48/64 for wing	Volume $\geqslant$ Volume$_{\text{ref}}$ Thickness $\geqslant$ Thickness$_{\text{min}}$	1 40 chord + 20 span
α	1	$C_{l_{\text{cruise}}} = C_{l_{\text{ref}}}$	1
β_{LE}, β_{TE}	2	$C_m \geqslant C_{m_{\text{min}}}$	1
Twist	4	$C_x \leqslant C_{x_{init}}$	1

Table 3: Optimization problem definition. Parameters in blue apply to wing optimization, while the morphing edges variables are highlighted in green.

**Concorde Navigation Map: http://afconcorde.free.fr/SSCroute.htm

The trim requirements are indirectly enforced in the form of a minimum C_{mz} (pitching moment coefficient). The constraint values are dictated by ADODG case 2 [††] for 2D cases, and by the baseline wing initial performance for 3D optimization. For these last studies, we also include a bending moment constraint to roughly ensure the structural feasibility of the wing without embedding a structural model in the analysis.

We also impose both volume and thickness constraints. The minimum cross-sectional area and internal volume values come from biconvex airfoil and wing illustrated in Sec. 3.1. The minimum thickness constraint is ∼1 mm from 10% to 90% of the chord and ∼0.1 mm closer to the edges, preventing the optimizer from crossing the upper and lower surfaces (as discussed by Drela [80]), while allowing "sharp" leading and trailing edges.

The objective function for multipoint cases is the weighted drag average for the different flight conditions, using the same approach as in previous work [54, 81]. We consider an optimization converged when the relative residual of first-order optimality conditions is less than 10^{-6}.

4 Results

The results of our study for both the 2D and 3D cases are discussed in this section. We initially optimize an airfoil at supersonic flight speed for both non-lifting and lifting conditions. The influence of the cruise Mach number, C_l, and the FFD control-point distribution is investigated. Following that, the problem is extended to simultaneously take into account multiple flight conditions, comparing the optimal fixed designs with morphing configurations and assessing the influence of different mission profiles. Then, we shift to full-wing optimization. We first investigate the effect of solely the twist variables in terms of drag minimization and framework manipulation capabilities, ultimately selecting the most suitable control points distribution. We then include shape variables in the 3D optimization and compare the single-point optimization performance with the morphing, multipoint configurations.

4.1 2D non-lifting minimum drag shape

To initially assess the optimization routine accuracy, we run a benchmark case, the drag minimization of a non-lifting airfoil in supersonic flow (Fig. 4), and we compare the final shape with the 2D Sears–Haack body as theoretical minimum-drag shape. The airfoil cross-sectional area is fixed (1% tolerance), while no thickness constraints are enforced. We use two different control point sets with 12 and 16 points respectively. We enforce symmetry between upper and lower surfaces, to avoid inconsistent shape modifications induced by machine-level numerical errors on C_l prediction.

We observe a rearward shift in the maximum thickness position along the longitudinal axis with respect to the theoretical optimum (Fig. 4(a)). This result follows the inviscid analysis by Palaniappan and Jameson [82], who suggest that the difference

[††]ADODG website: https://sites.google.com/view/mcgill-computational-aerogroup/adodg

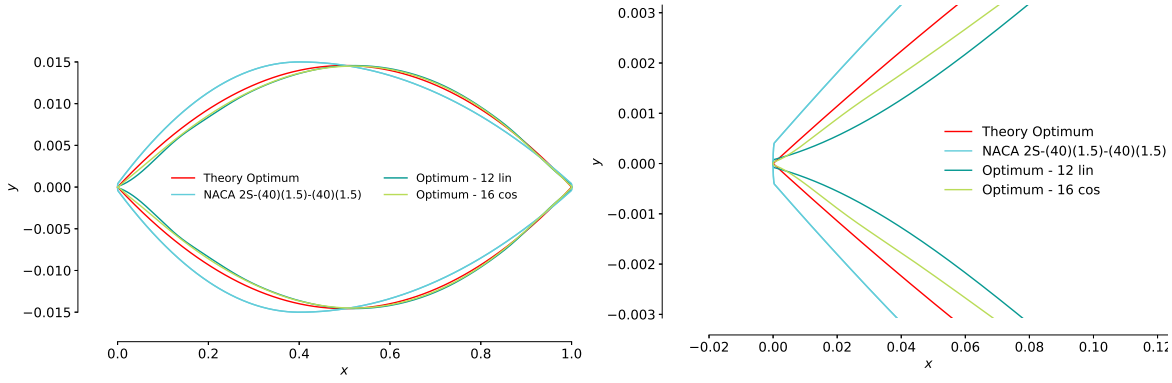

(a) Shape comparison

(b) LE detail

Figure 4: Comparison between the optimal shape for C_l=0 and the 2D Sears–Haack body (a), and a detail of shape parametrization influence on the leading edge (b).

from theoretical optimum comes from the presence of a shockwave not predicted by the linearized analytical model. The CFD analysis shows a reduction in the leading-edge shock intensity in the optimal airfoil, coming from a more gradual slope in the fore section, as shown in Fig. 4(b). The drag decreases by 10.6% and 11.5% for 12-DV and 16-DV cases, respectively. The more refined parametrization further reduces the nose radius and exhibits a more limited chordwise propagation of the local deformation at the leading edge.

4.2 2D single-point supersonic optimization

We now extend our investigation to the influence of C_l constraint and freestream Mach on the optimized layout.

Figure 5(a) shows the optimization results for fixed supersonic flight conditions (Table 3) with varying C_l constraint. The thickness distribution for different cases has negligible variations and is consistent with the non-lifting case just discussed. On the other hand, airfoil camber increases with C_l, with a shift in the maximum height position from 65% to 54% of the chord and the appearance of a "bump" between 15% and 40% of the chord. The optimizer diverges from the symmetrical shape and reduces the angle of attack compared to linear analytical model results, as shown in Table 4.

The effects of a varying freestream velocity at constant C_l are shown in Fig. 5(b). In this case, the bump on the camber line increases with decreasing speed. Such modification is justified by the minimization of shock intensity and subsonic flow regions close to the front lower surface, ultimately reducing the wave drag. With this brief analysis, we further prove how the use of a high-fidelity tool improves the performance of a well-known and theoretically-investigated shape such as the 2D minimum-drag section.

Having highlighted the impact of physical factors on supersonic airfoil optimization, we shift the focus on the shape parametrization, to ensure that the initial airfoil choice had a minimum effect on the final shape. Therefore, we compare a set of FFD grids with different design variables number in Fig. 6, from 12 to 20 stations (with two control

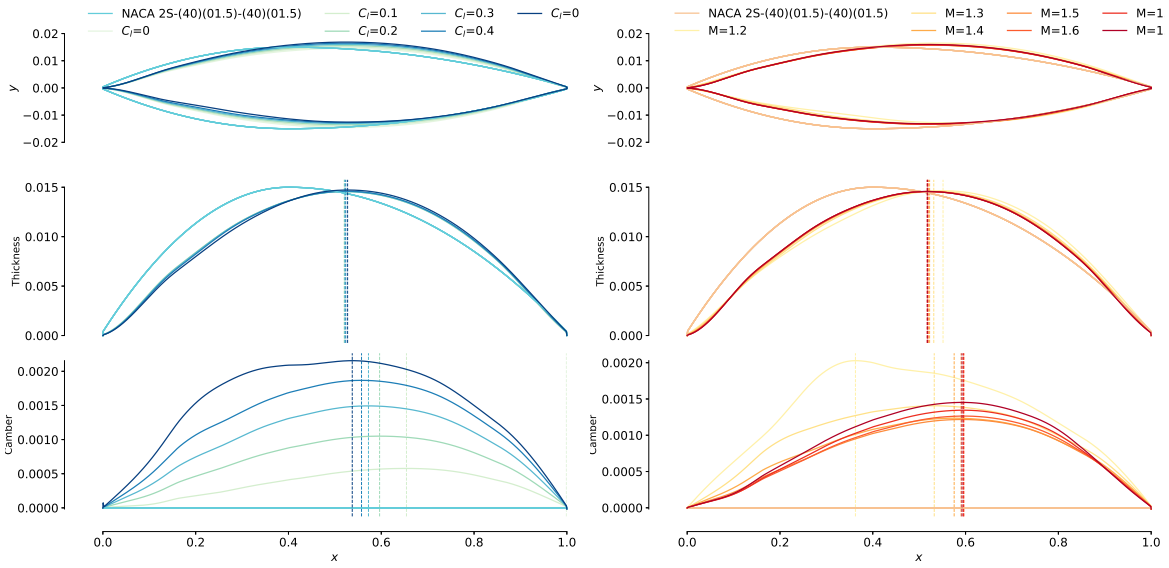

(a) Fixed speed and altitude (b) Fixed C_l

Figure 5: Optimization results for (a) varying C_l at $M = 1.45$, 45,000 ft and (b) varying cruise Mach at fixed C_l=0.236.

$C_l =$	0	0.1	0.2	0.3	0.4	0.5
α_{optimal}	0.0°	1.49°	2.97°	4.43°	5.84°	7.17°
α_{theory}	0.0°	1.51°	3.01°	4.52°	6.02°	7.52°

Table 4: Angle of attack for optimal layouts with varying C_l and comparison with linearized supersonic theory.

points at each station for upper and lower surface respectively), and different chordwise distribution. It turns out that the 16 DV, cosine-spaced distribution offers the best accuracy with a relatively small computational time penalty, if compared to FFD grids with a higher number of control points. The optimization runs are performed on an HPC cluster equipped with Haswell architecture compute nodes (12-core 2.5 GHz Intel Xeon E5-2680v3 processors), using 12 processors for each case.

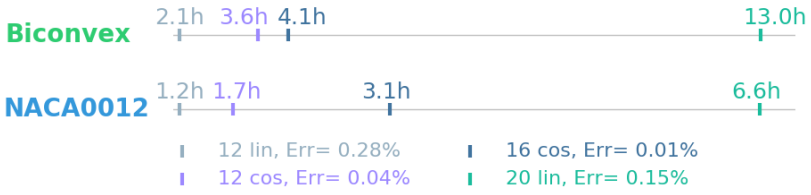

Figure 6: Computational time and discrepancy for a single-point supersonic optimization using different FFD grids.

To further test the framework robustness, we optimize the RAE2822 and NACA66-

206 sections with the same settings. The shape, pressure distribution, and drag coefficient, are shown in Fig. 7(a), Fig. 7(b), and Table 5, and highlight an excellent match between the different cases. The final results differ by a maximum of 0.06 drag counts (0.025%) and a minimum discrepancy (up to 0.8°) in the optimal angle of attack, most likely due to the mesh distortion. This comparison further supports the assumption of unimodality for the supersonic optimization problem.

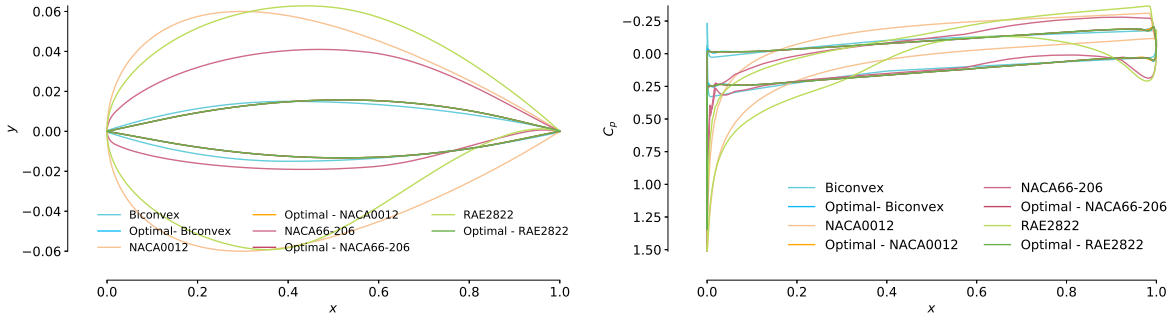

(a) Shape comparison

(b) Pressure distribution comparison

Figure 7: Drag minimization of an airfoil at $M = 1.45$, 45,000 ft, and $C_l = 0.236$, starting from NACA 2S-(40)(1.5)-(40)(1.5), NACA 0012, NACA 66-206, and RAE 2822.

The drag reduction in the order of 50%–80% shown in Table 5 for NACA 4 and 6 digit, and RAE airfoils comes from the initial poor performance of these layouts at supersonic speed.

Baseline airfoil	Initial C_d	Final C_d	ΔC_d	α
NACA 2S-(40)(1.5)-(40)(1.5)	253.80	240.74	−5.14%	3.53°
NACA 0012	1173.94	240.76	−79.49%	3.54°
NACA 66-206	485.15	240.70	−50.38%	3.45°
RAE 2822	1100.56	240.72	−78.12%	3.46°

Table 5: Results for single-point, supersonic optimization starting from different initial airfoils reported in Fig. 7.

4.3 2D multipoint optimization

We now move on to multipoint airfoil optimization studies to minimize the drag penalty of a high-speed airfoil at both transonic and subsonic speeds.

As a first test case, we simultaneously optimize a baseline wing section for supersonic, transonic and subsonic reference conditions while enforcing equally-weighted flight segments in the objective function. This problem formulation is an extreme test case useful to prove optimization robustness, highlight the design tradeoff features and ultimately maximize the benefits of the airfoil morphing capabilities. In Fig. 8, we compare the results of this "equal-weights" optimization problem both without

and with the addition of edges deflection variables. The selected baseline shape is a NACA 66-206 section.

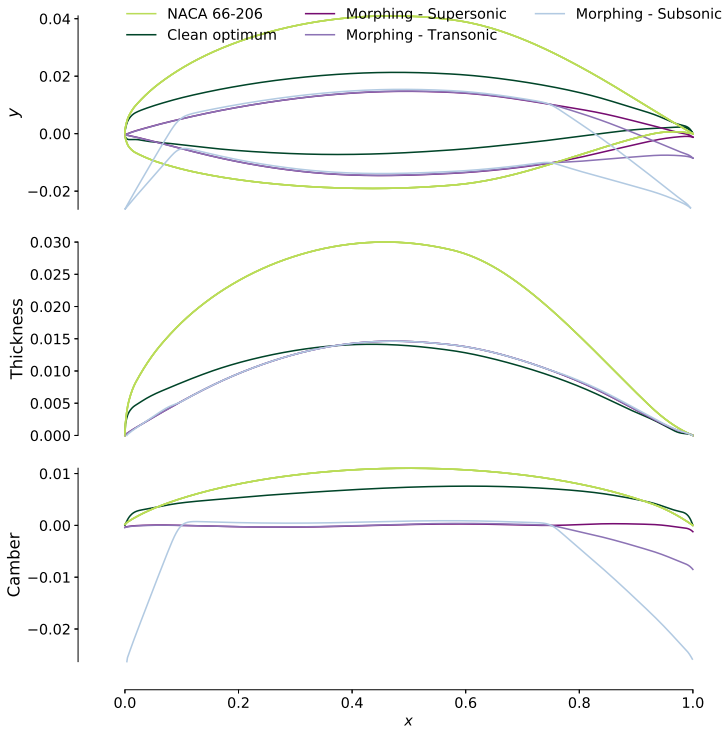

Figure 8: Shape comparison between the fixed shape and the morphing airfoil multipoint optimization - equally-weighted flight segments.

With no edge deflection allowed, the optimizer converges to a compromise between the typical features of supersonic and subsonic airfoils. The optimal layout features a thick, cambered round leading edge. A sharper nose would indeed lead to separation and higher drag at the low-speed, high-C_l subsonic flight condition. Conversely, the trailing edge kink and pitching-down tail resemble supercritical, transonic airfoils features. The thickness distribution is comparable to the typical parabolic distribution of supersonic airfoils, except for the nose section.

	Supersonic	Transonic	Subsonic
Baseline (NACA 66-206)	485.15	618.55	81.82
Fixed shape optimum	307.54	264.76	81.65
Morphing optimum	243.23	263.80	73.74

Table 6: Baseline and optimized shape drag (in counts) for multipoint optimization, comparing fixed shape and morphing airfoil cases with equally-weighted flight segments.

The performance tradeoff reported in Table 6 highlights how the supersonic drag is more than 77 drag counts (32%) higher than the corresponding single-point optimization results. In comparison, the subsonic drag is only 0.2 drag counts off the

baseline. The cross-sectional area reduction from the initial NACA66-206 geometry is undoubtedly contributing to the overall performance improvement.

The introduction of morphing capabilities relaxes the tradeoff between different design conditions by decoupling the main optimization problem into three, almost-independent, drag minimization problems. At the supersonic speed, C_d is now only 1% higher than the pure supersonic optimization results. This improvement is owing to the reduction of the leading-edge radius, which results in a lower leading-edge shock strength. At the same time, thanks to the deflection of both leading and trailing edges ($-15.4°$ and $5.7°$ respectively), the subsonic drag is reduced by 9.7% relative to the fixed-shape airfoil results. The higher surface curvature at the virtual hinges location, together with the reduction of the local angle of attack at the leading edge, minimize the disadvantages of using a sharp airfoil at low speeds. The negligible performance improvement at the transonic flight condition suggests that the leading-edge radius has a minor influence on the performance at this specific flight condition.

Results discrepancy			
Fixed	Supersonic	C_d	**0.02%**
		α	1.12%
	High transonic	C_d	**0.04%**
		α	1.67%
	Subsonic	C_d	**1.29%**
		α	2.04%
Morphing	Supersonic	C_d	**0.03%**
		α	10.18%
		β_{LE}/β_{TE}	20.00%/428%*
	High transonic	C_d	**0.07%**
		α	14.83%
		β_{LE}/β_{TE}	53.3%/764%*
	Subsonic	C_d	**0.54%**
		α	16.85%
		β_{LE}/β_{TE}	2.23%/16.54%

Table 7: Results relative discrepancy for the multipoint optimization in Fig. 9, starting from NACA 2S-(40)(1.5)-(40)(1.5) and NACA 66-206.
* the absolute deflection discrepancy is still in the order of 1°.

Given the insight provided by this first multipoint optimization example, we assess the potential of our optimization strategy when applied to a more realistic optimization problem. Data in Table 7 and Fig. 9 refer to a drag minimization case where the flight conditions are weighted according to an ideal CDG-JFK route with high-transonic ($M = 1.15$) overland segment, as presented in Sec. 3.3. We also check the unimodality of the problem by showing how two different initial airfoils, NACA2S-(40)(1.5)-(40)(1.5) and NACA66-206, converge with minimal discrepancy (max ΔC_d=0.54%) to the same results. We consider the relative mismatch between the angle of attack

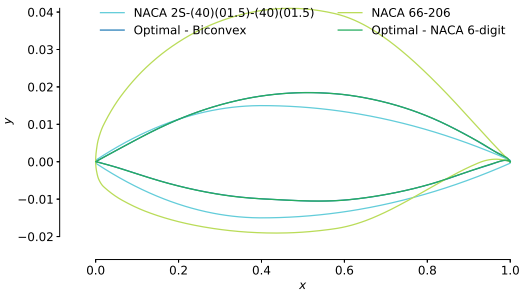

(a) Fixed optimized shape

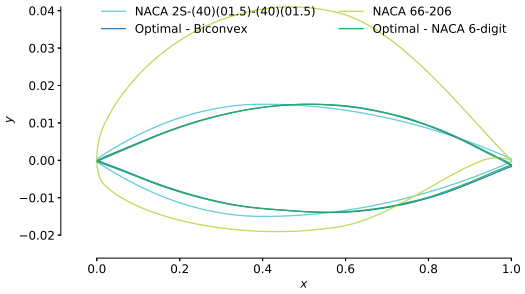

(b) Morphing at the supersonic flight condition.

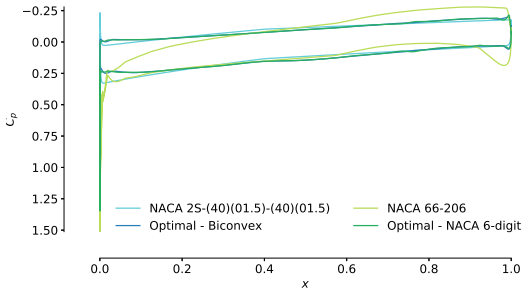

(c) Pressure distribution at the supersonic flight condition.

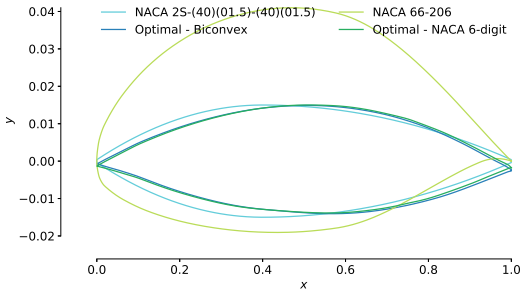

(d) Morphing at the transonic flight condition.

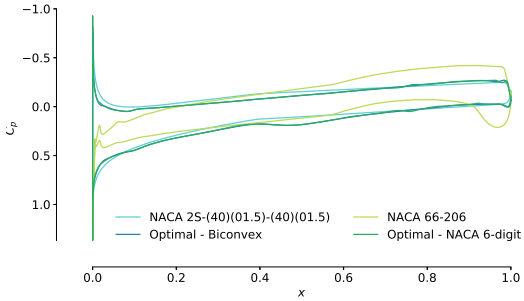

(e) Pressure distribution at the transonic flight condition.

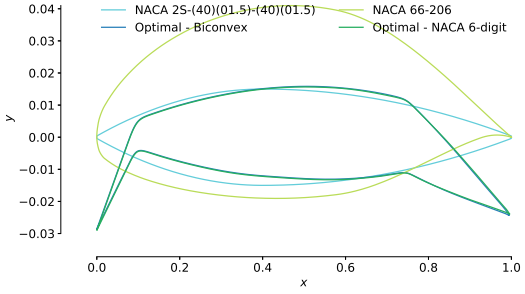

(f) Morphing at the subsonic flight condition.

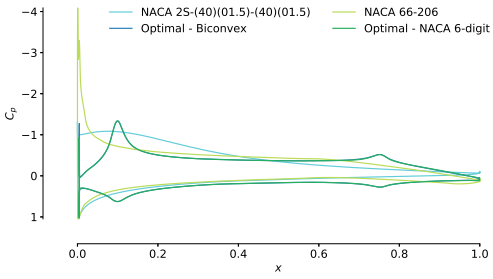

(g) Pressure distribution at the subsonic flight condition.

Figure 9: Shape comparison for fixed and morphing airfoil multipoint optimization starting from NACA 2S-(40)(1.5)-(40)(1.5) and NACA 66-206. Flight segments weighted for CDG-JFK flight route.

and the edge deflections, respectively, as a result of different FFD grid distortion when starting from different geometries. These α and β discrepancies compensate each other to return identical pressure distributions, as shown in Fig. 9.

ΔC_d	Supersonic	Transonic	Subsonic
Fixed	-4.1%	-5.9%	-21.4%
Morphing	-5.1%	-6.7%	-86.9%

Table 8: Performance comparison between fixed and morphing airfoil optimization along the reference CDG-JFK route, for cases reported in Fig. 9. Reference initial drag refers to NACA2S-(40)(1.5)-(40)(1.5).

As shown in Fig. 9, the fixed-shape optimum is now much closer to an optimal supersonic shape, exhibiting some of the features discussed for the previous case. In particular, the fixed shape in Fig. 9(a) has a positive camber if compared to the quasi-symmetrical, morphing airfoil in Fig. 9(b). Moreover, we observe the twisted-down trailing edge previously shown in Fig. 8. The morphing-shape optimum has once again a superior performance for all the flight conditions, as reported in Table 8, where the reference is the NACA2S-(40)(1.5)-(40)(1.5) airfoil. The drag improvements at the subsonic flight condition are explained by the initial poor performance of the biconvex airfoil at low speed.

In the last 2D case study, we compare two fixed shapes, multipoint optimal airfoils, using different transonic flight conditions for the 10% overland flight segment. Despite such a small relative weight, the final layouts show a discernible difference in shape (Fig. 10). While the upper surfaces are overlapping, the forward shift in maximum thickness position and the rearward shift of maximum camber location lead to a different lower surface curvature. For the "conventional" ($M_{\text{overland flight}}$=0.95) optimization case, the algorithm minimizes the supercritical flow regions over the pressure side. The higher freestream speed for the "boomless" ($M_{\text{overland flight}}$=1.15) case implies a different optimal pressure distribution and consequently, a higher curvature in the rearmost part of the lower surface.

C_d	Supersonic	High transonic	Transonic	Subsonic
NACA 2S-(40)(1.5)-(40)(1.5)	253.80	273.66	310.82	569.25
"Conventional" optimum	244.23	260.79	277.57	434.87
"Boomless" optimum	243.31	257.52	292.95	447.13

Table 9: Airfoil optimization results for CDG-JFK route considering different overland flight conditions (gray: not included in optimization stencil).

The above-mentioned shape discrepancies lead to quantifiable drag benefits, as highlighted in Table 9. Our high-fidelity optimization tool demonstrates the capability to capture the complex phenomena of transonic and supersonic flows and maximize the performance with minor but essential shape adjustments.

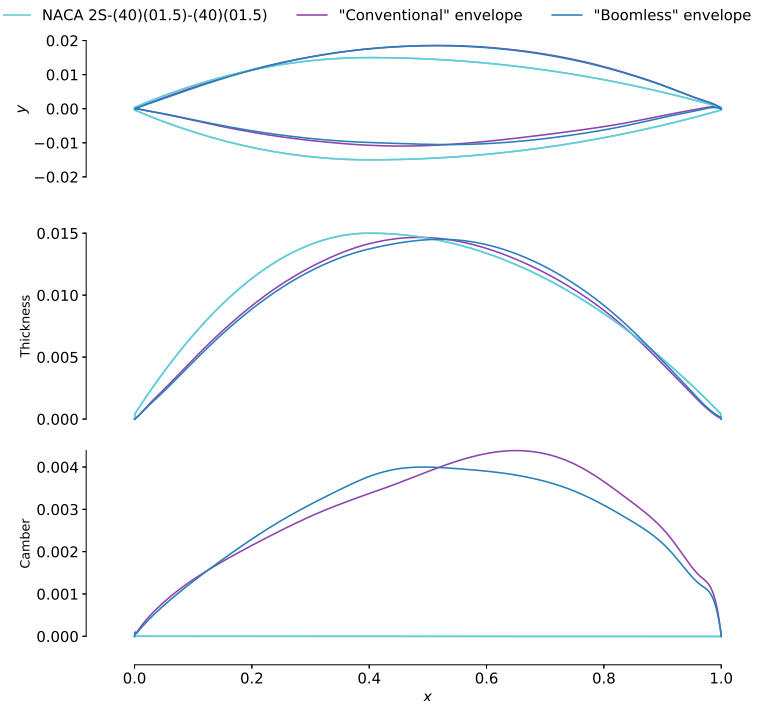

Figure 10: Shape comparison for two fixed airfoils optimized for CDG-JFK route, considering transonic (conventional) and high-transonic (boomless) overland cruise speed respectively.

4.4 3D single-point optimization

We now shift our focus to the full-wing drag minimization problem, using the baseline geometry described in Sec. 3.1. As done for the airfoil, we first investigate the performance improvements obtainable for supersonic regime only and then extend the problem to the transonic and subsonic regimes. As a first design case, we perform a single-point supersonic optimization with just the angle of attack and the twist design variables. We investigate the impact of these variables and identify the best control-point distributions for our design problem.

Initial C_d: 207.05		
Twist variables	Optimum C_d	ΔC_d
3	194.72	-6.0%
5	194.25	-6.2%
7	193.66	-6.5%

Table 10: Results for twist-only optimization of a planar wing for the supersonic flight condition. The pitching moment constraint is active for this design problem.

The reference wing presents a lift distribution close to elliptical, given by the spanwise chord distribution of the trapezoid planform. Despite it being the ideal force

distribution for minimum induced drag, the final layout presents an unexpected lift trend that diverges from baseline. Figure 11(a) shows that, regardless of the selected parametrization, the optimizer increases the sectional lift close to the root section and then non-linearly decreases it along the outboard direction. Local lift values flatten in the proximity of the wingtip. This behavior is less evident on the baseline wing due to smaller local α and is owing to the presence of a tip vortex at the straight, large tip.

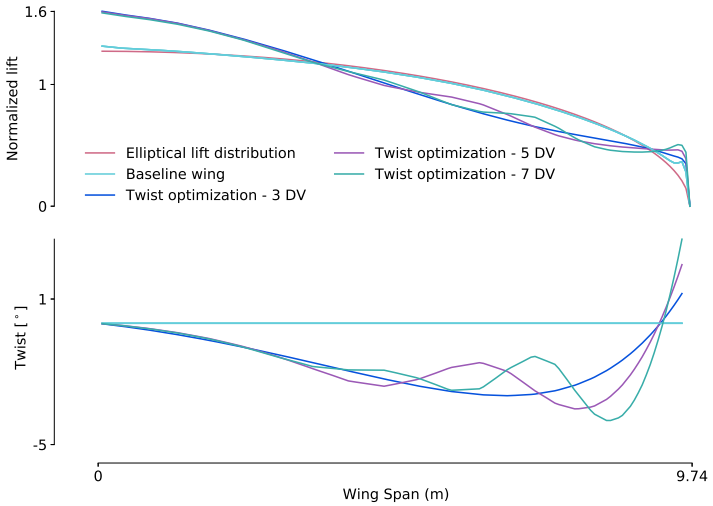

Figure 11: Lift and twist profiles for twist-only, supersonic optimization of a planar wing, using 3, 5, and 7 twist design variables respectively.

Figure 11(b) provides insights on the final wing shape. The general trend is to linearly decrease the twist on the 30% innermost wing section and, conversely, to pitch up the wing at the very tip. This, coupled with an increase in the angle of attack, enables the matching of the C_L constraint while minimizing the local α in the center wing section. It is also evident how an increase in uniformly-spaced twist variables reduces the wing profile smoothness, introducing an unwanted twist oscillation. Given this concern and the minimal drag benefits when using a higher number of twist variables (Table 10), we opt to use three spanwise twist sections for the following optimization studies.

If unconstrained, the optimizer would increase the pitching down attitude with detrimental effects on trim drag, looking at the overall aircraft design. Therefore, the imposed pitching moment constraint is essential for this optimization case to provide a feasible final layout. Despite these constraints, the optimal layout shows a 6% drag decrease thanks solely to the manipulation of the three twist variables.

We then increase the design case complexity by including the local shape variables in the problem, with results highlighted in Fig. 12. Compared to the twist-only case, the lift distribution shows a similar non-linear trend, with higher sectional lift between 15% and 60% of the span and, conversely, lower lift close to the root and the tip. The twist distribution has a parabolic trend, with a minimum of -5° close to the 50% of the wingspan. The improved performance of this configuration is probably due to the propagation of the leading-edge shockwave outboard from the root section. The

high-pressure zone over the lower surface, magnified by the local shape and high angle of attack in the proximity of the root, has beneficial effects on the overall performance despite the local drag penalty. The central sections of the low-aspect-ratio wing primarily benefit from the shock-induced overpressure propagating along the lower surface. These sections then need a lower local α to generate the target lift, minimizing both the wave and lift-induced drag of the overall configuration.

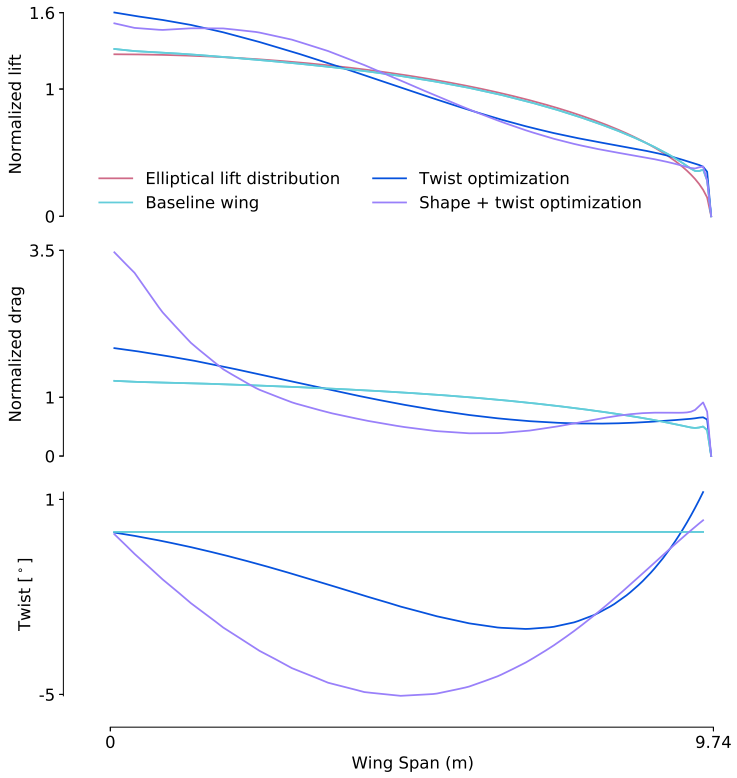

Figure 12: Spanwise lift, drag and twist distributions for the twist-only and twist+shape single-point, supersonic wing optimization case.

Initial C_d: 207.05			
Design variables	Optimum C_d	ΔC_d	α
Twist only	194.72	-6.0%	$4.42°$
Twist and shape	154.74	-25.2%	$4.75°$

Table 11: Results comparison between the twist-only optimization and the twist+shape single-point, supersonic wing optimization case. As for the previous case, the pitching moment constraint is active.

Compared to the reference planar wing, our novel supersonic wing layout shows a 25% drag decrease, Table 11. Such performance improvement is magnified by the sub-optimal performance of the simple baseline geometry. Nevertheless, the optimal layout

sets an upper limit in the drag reduction for further full-configuration or aerostructural studies. Concerns involving the reduced optimized wing off-design performance (discussed in Sec. 4.5) and design feasibility in terms of structure and manufacturing could be addressed in future work involving more tightly-constrained design problems.

4.5 3D multipoint optimization

Finally, we present the last and most complex optimization problem of this study. We perform a multipoint wing optimization for supersonic, transonic and subsonic flight conditions, including morphing capabilities. The geometry constraints are the same we enforced for the single-point case. For the lower-speed flight conditions, the pitching and bending moment constraints on lower and upper values are set to match baseline wing values. The relative weights of the flight conditions in the optimization refer to the previously discussed CDG-JFK route, with "conventional" overland transonic flight.

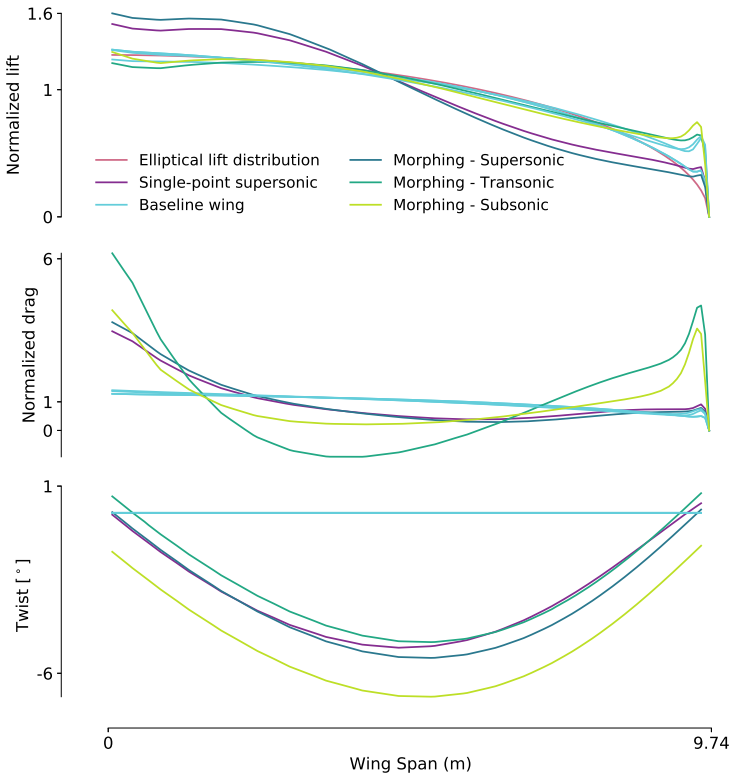

Figure 13: Spanwise lift, drag, and twist distributions for the multipoint morphing wing optimization. The flight segments are weighted for a CDG–JFK mission profile.

The lift, drag, and twist distribution for multipoint optimized wing are compared to the single-point supersonic drag-minimization results in Fig. 13. For the supersonic flight condition, the lift and drag distributions of the two optimization cases exhibit similar trends. The morphing optimum shows a 5% lift increase at the inboard section and an average 14% decrease at the tip compared to the single point case. The twist

differences are between 0.5–0.8% in the wing outboard half. At the lower speeds, the optimizer maintains the lift distribution close to the elliptical reference, except for the already mentioned tip vortex influence on the outermost 10% of the span.

Flight condition	Initial C_d	Optimum C_d	ΔC_d	α	β_{LE}	β_{TE}
Supersonic	207.05	156.29	−24.5%	4.89°	0.83°	−0.01°
Transonic	207.45	53.30	−74.3%	4.30°	−1.05°	3.13°
Subsonic	305.09	87.97	−71.2%	8.37°	−15.58°	0.58°

Table 12: Drag, angle of attack, and edge deflections for the multipoint wing optimization with morphing capabilities.

The supersonic drag is consistent with the single-point optimization case. At transonic speed, the drag distribution is highly non-linear, with a 440% drag increase at root-section compared to the baseline, compensated by a drag reduction of a similar order of magnitude in the central wing section. For these specific wing planform and cruise conditions, the drag minimization at supersonic cruise is dominated by the improvements at the subsonic and transonic flight conditions when morphing capabilities are enabled, as reported in Table 12. Considering the biconvex wing section we selected for the baseline airfoil, this is in line with the NACA 2S-(40)(1.5)-(40)(1.5) 2D morphing optimization cases discussed in Sec. 4.3.

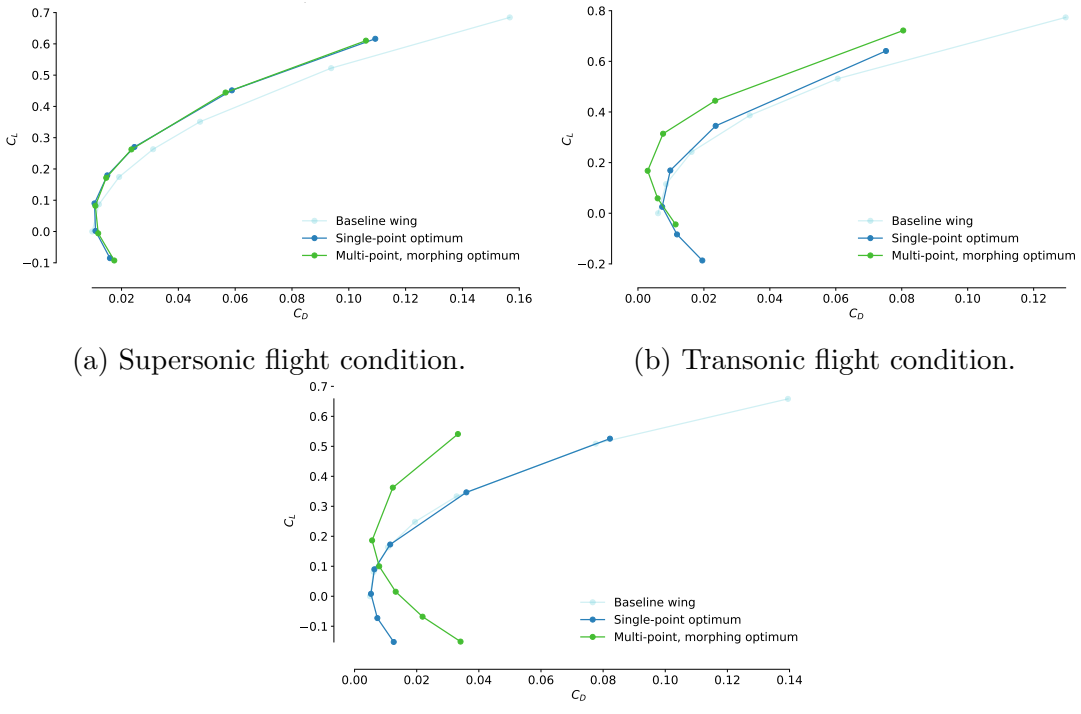

(a) Supersonic flight condition.

(b) Transonic flight condition.

(c) Subsonic flight condition.

Figure 14: C_L vs. C_D polars for single-point and multipoint optimized wings.

The advantages that come from using morphing edges are further illustrated in Fig. 14. At the transonic speed, Fig. 14(b), the morphing design shows a drag advantage up to 70% at $C_L = 0.17$ with respect to the reference low-aspect-ratio, planar trapezoid wing. Such an efficiency increase confirms the expectations for this study, as we aim to minimize the drag penalty of a supersonic aircraft when flying at lower design speeds. Likewise, at the subsonic flight condition, the high edge deflection (see Table 12) leads to C_L/C_D benefits for $C_L > 0.1$.

The negative twist and edge deflections of both wing designs induces a negative C_L at low angles of attack. However, this issue could be resolved by assuming a positive wing mounting angle on the fuselage. This would further ensure that the design lift is achieved at an angle of attack lower than wing-only values, minimizing fuselage drag. In the last instance, we restate that β_{LE} and β_{TE} have been kept constant during the α sweep plotted in Fig. 14. Allowing the edges to adapt to a range of angles of attack by performing an optimization could result in further wing performance improvement.

5 Conclusions

In this paper, we present a series of CFD-based aerodynamic shape optimization studies for supersonic aircraft airfoils and wings, considering supersonic, transonic, and subsonic conditions. We use the MACH framework to minimize the drag subject to lift, pitching moment, bending moment, and geometry constraints.

In the airfoil optimization studies, we investigate the influence of control points distribution, freestream conditions, and design lift coefficient on the final shape for supersonic flight conditions. We improve the performance of a typical biconvex airfoil by 5.5%, while enforcing geometry, lift, and pitching moment constraints. We then present a selection of multipoint optimization studies aimed at minimizing the drag penalty at lower speeds without compromising the supersonic performance. We improve the same reference airfoil performance at supersonic, transonic, and subsonic speed by 5.1%, 6.7%, and 86.9%, respectively. The improvements at low-speed are magnified by the poor performance of the baseline configuration at subsonic flight conditions. We demonstrate how deflecting edges relax the tradeoffs and improve the performance at all flight conditions. The results support the unimodality hypothesis for this optimization problem.

For the full-wing optimization, we define a baseline planar, trapezoid-planform wing, and investigate how twist and shape modifications affect drag at supersonic speed. Using twist design variables results in a drag reduction of 6%, and adding shape variables reduces it further, by a total of 25%. The lift distribution is tailored to minimize the wave and lift-induced drag jointly, and is significantly different from an elliptical distribution. Finally, we perform a multipoint shape optimization on the same wing, including leading and trailing edge deflection design variables. We show how the supersonic performance matches the single-point cases, while the drag for the transonic and subsonic flight conditions is reduced by 74.3% and 71.2%, respectively, relative to the baseline supersonic design.

The case studies mark a significant step forward in terms of accuracy and design

capability. The results we discuss provide a qualitative and quantitative insight into the numerical and physical factors that affect the supersonic airfoil and wing design optimization. Ultimately, this work highlights the usefulness of RANS-based ASO in the exploration of design tradeoffs between different flight regimes.

Acknowledgments

The authors would like to thank Philip Roe for providing crucial physical insight in the interpretation of our wing optimization results. The computations were performed on the Flux HPC cluster at the University of Michigan Center of Advanced Computing. This research was partially funded by TU Delft's Justus and Louise van Effen research grant.

References

[1] Anderson, J. D., *Fundamentals of Aerodynamics*, McGraw–Hill, 1991.

[2] Murakami, A., "Silent supersonic technology demonstration program," *Proceedings on 25th International Council of the Aeronautical Sciences*, 2006.

[3] Sturdza, P., "Extensive Supersonic Natural Laminar Flow on the Aerion Business Jet," *Proceedings of the 45th AIAA Aerospace Sciences Meeting and Exhibit*, Reno, NV, 2007. doi:10.2514/6.2007-685.

[4] Vermeersch, O., Yoshida, K., Ueda, Y., and Arnal, D., "Natural laminar flow wing for supersonic conditions - Wind tunnel experiments, flight test and stability computations," *Progress in Aerospace Sciences*, 2015, pp. 64–91. doi:10.1016/j.paerosci.2015.07.003.

[5] Frederick, M. A., W, D. B., Garzon, G., and Matisheck, J., "Flight tests of a supersonic natural laminar flow airfoil," *Measurement Science and Technology*, Vol. 26, No. 6, 2015. doi:https://doi.org/10.1088%2F0957-0233%2F26%2F6%2F064003.

[6] Skinner, S., and Zare-Behtash, H., "State-of-the-art in aerodynamic shape optimisation methods," *Applied Soft Computing*, Vol. 62, 2018, pp. 933–962. doi:10.1016/j.asoc.2017.09.030.

[7] Sun, Y., and Smith, H., "Review and prospect of supersonic business jet design," *Progress in Aerospace Sciences*, Vol. 90, 2017, pp. 12–38. doi:10.1016/j.paerosci.2016.12.003.

[8] Hicks, R. M., Murman, E. M., and Vanderplaats, G. N., "An assessment of airfoil design by numerical optimization," Tech. rep., NASA TM X-3092, July 1974.

[9] Von Karman, T., "Supersonic aerodynamics—principles and applications," *Journal of the Aeronautical Sciences*, Vol. 14, No. 7, 1947, pp. 373–409. doi:10.2514/8.1394.

[10] Munk, M. M., "The reversal theorem of linearized supersonic airfoil theory," *Journal of Applied Physics*, Vol. 21, No. 2, 1950, pp. 159–161. doi:10.1063/1.1699616.

[11] Tsien, H.-S., and Baron, J. R., "Airfoils in slightly supersonic flow," *Journal of the Aeronautical Sciences*, Vol. 16, No. 1, 1949, p. 55. doi:10.2514/8.11725.

[12] Reuther, J., Cliff, S., Hicks, R., and Van Dam, C., "Practical design optimization of wing/body configurations using the Euler equations," *10th Applied Aerodynamics Conference*, 1992, p. 2633. doi:10.2514/6.1992-2633.

[13] Reuther, J., and Jameson, A., "Supersonic wing and wing-body shape optimization using an adjoint formulation," Tech. rep., NASA, 1995.

[14] Reuther, J., Alonso, J. J., Rimlinger, M. J., and Jameson, A., "Aerodynamic shape optimization of supersonic aircraft configurations via an adjoint formulation on distributed memory parallel computers," *Computers & Fluids*, Vol. 28, No. 4, 1999, pp. 675–700. doi:10.1016/S0045-7930(98)00050-4.

[15] Kim, H.-J., Sasaki, D., Obayashi, S., and Nakahashi, K., "Aerodynamic optimization of supersonic transport wing using unstructured adjoint method," *AIAA Journal*, Vol. 39, No. 6, 2001, pp. 1011–1020.

[16] Jameson, A., "Aerodynamic Design via Control Theory," *Journal of Scientific Computing*, Vol. 3, No. 3, 1988, pp. 233–260. doi:10.1007/BF01061285.

[17] Cliff, S. E., Reuther, J. J., Saunders, D. A., and Hicks, R. M., "Single-Point and Multipoint Aerodynamic Shape Optimization of High-Speed Civil Transport," *Journal of Aircraft*, Vol. 38, No. 6, 2001, pp. 997–1005.

[18] Herrmann, U., and Orlowski, M., "Numerical Aerodynamic Optimization Study for a Supersonic Aircraft," *New Results in Numerical and Experimental Fluid Mechanics*, Springer, 1997, pp. 189–196. doi:10.1007/978-3-322-86573-1_24.

[19] Van der Velden, A., "Supersonic Aircraft Shape Optimization," *New Design Concepts for High Speed Air Transport*, Springer, 1997, pp. 237–250. doi:10.1007/978-3-7091-2658-5_16.

[20] Grenon, R., "Numerical optimization in aerodynamic design with application to a supersonic transport aircraft," *Proceedings of International Workshops on Numerical Simulation Technology for Design of Next Generation Supersonic Civil Transport (SST-CFD Workshop)*, 1998, p. 88.

[21] Lovell, D., "European research to reduce drag for supersonic transport aircraft," *Aerodynamic Drag Reduction Technologies*, Springer, 2001, pp. 117–132. doi:10.1007/978-3-540-45359-8_14.

[22] von Reith, D., "Experience and Potential of Multidisciplinary Optimization Tools on Supersonic Aircraft," Tech. rep., SAE Technical Paper, 1997.

[23] Laban, M., "Multi-disciplinary analysis and optimisation of supersonic transport aircraft wing planforms," *10th AIAA/ISSMO Multidisciplinary Analysis and Optimization Conference*, 2004, p. 4542. doi:10.2514/6.2004-4542.

[24] Laban, M., and Herrmann, U., "Multi-Disciplinary Analysis and Optimisation Applied to Supersonic Aircraft Part 1: Analysis Tools," *48th AIAA/ASME/ASCE/AHS/ASC Structures, Structural Dynamics, and Materials Conference*, 2007, p. 1857. doi:10.2514/6.2007-1857.

[25] Herrmann, U., and Laban, M., "Multi-Disciplinary Analysis and Optimisation Applied to Supersonic Aircraft Part 2: Application & Results," *48th AIAA/ASME/ASCE/AHS/ASC Structures, Structural Dynamics, and Materials Conference*, 2007, p. 1858. doi:10.2514/6.2007-1858.

[26] Jameson, A., Martinelli, L., Cliff, S., and Thomas, S., "Aerodynamic shape optimization of transonic and supersonic aircraft configurations," *43rd AIAA Aerospace Sciences Meeting and Exhibit*, Reno, Nevada, 2005.

[27] Choi, S., Alonso, J. J., and Kroo, I. M., "Two-level multifidelity design optimization studies for supersonic jets," *Journal of Aircraft*, Vol. 46, No. 3, 2009, p. 776. doi:10.2514/1.34362.

[28] Sasaki, D., Morikawa, M., Obayashi, S., and Nakahashi, K., "Aerodynamic Shape Optimization of Supersonic Wings by Adaptive Range Multiobjective Genetic Algorithms," *Evolutionary Multi-Criterion Optimization*, 2001, pp. 639–652. doi:10.1007/3-540-44719-9_45.

[29] Obayashi, S., and Sasaki, D., "Self-organizing map of Pareto solutions obtained from multiobjective supersonic wing design," *AIAA Paper* 2002-0991, 2002.

[30] Seto, N., "Multi-Disciplinary Design Optimization of Supersonic Transport Wing Using Surrogate Model," *27th International Congress of the Aeronautical Sciences, Nice, France, ICAS-Paper*, 2010.

[31] Kim, Y., Jeon, Y.-H., and Lee, D.-H., "Multi-objective and multidisciplinary design optimization of supersonic fighter wing," *Journal of Aircraft*, Vol. 43, No. 3, 2006, pp. 817–824. doi:10.2514/1.13864.

[32] Sasaki, D., Obayashi, S., and Kim, H.-J., "Evolutionary algorithm vs. adjoint method applied to sst shape optimization," *The Annual Conference of CFD Society of Canada, Waterloo*, 2001.

[33] Martins, J. R. R. A., Alonso, J. J., and Reuther, J. J., "High-Fidelity Aerostructural Design Optimization of a Supersonic Business Jet," *Journal of Aircraft*, Vol. 41, No. 3, 2004, pp. 523–530. doi:10.2514/1.11478.

[34] Nadarajah, S. K., Jameson, A., and Alonso, J. J., "Sonic Boom Reduction using an Adjoint Method for Wing-Body Configurations in Supersonic Flow," *AIAA Paper* 2002-5547, 2002.

[35] Choi, S., Alonso, J. J., Kroo, I. M., and Wintzer, M., "Multifidelity Design Optimization of Low-Boom Supersonic Jets," *Journal of Aircraft*, Vol. 45, No. 1, 2008, pp. 106–118.

[36] Alonso, J. J., and Colonno, M. R., "Multidisciplinary Optimization with Applications to Sonic-Boom Minimization," *Annual Review of Fluid Mechanics*, Vol. 44, No. 1, 2012, pp. 505–526. doi:10.1146/annurev-fluid-120710-101133.

[37] Kroo, I., Willcox, K., March, A., Haas, A., Rajnarayan, D., and Kays, C., "Multifidelity analysis and optimization for supersonic design," Tech. rep., NASA/CR-2010-216874, 12 2010.

[38] Allison, D., Morris, C., Schetz, J., Kapania, R., Sultan, C., Deaton, J., and Grandhi, R., "A multidisciplinary design optimization framework for design studies of an efficient supersonic air vehicle," *12th AIAA Aviation Technology, Integration, and Operations (ATIO) Conference and 14th AIAA/ISSMO Multidisciplinary Analysis and Optimization Conference*, 2012, p. 5492. doi:10.2514/6.2012-5492.

[39] Geiselhart, K., Ozoroski, L., Fenbert, J., Shields, E., and Li, W., "Integration of multifidelity multidisciplinary computer codes for design and analysis of supersonic aircraft," *49th AIAA Aerospace Sciences Meeting Including the New Horizons Forum and Aerospace Exposition*, 2011, p. 465. doi:10.2514/6.2011-465.

[40] Feng, X., Li, Z., and Song, B., "Research of low boom and low drag supersonic aircraft design," *Chinese Journal of Aeronautics*, Vol. 27, No. 3, 2014, pp. 531–541. doi:10.1016/j.cja.2014.04.004.

[41] Kiyici, F., and Aradag, S., "Design and Optimization of a Supersonic Business Jet," *22nd AIAA Computational Fluid Dynamics Conference*, 2015, p. 3064. doi:10.2514/6.2015-3064.

[42] Sun, Y., and Smith, H., "Supersonic Business Jet Conceptual Design in a Multidisciplinary Design Analysis Optimization Environment," *2018 AIAA/ASCE/AHS/ASC Structures, Structural Dynamics, and Materials Conference*, 2018, p. 1651. doi:10.2514/6.2018-1651.

[43] Hu, R., Jameson, A., and Wang, Q., "Adjoint-based aerodynamic optimization of supersonic biplane airfoils," *Journal of Aircraft*, Vol. 49, No. 3, 2012, pp. 802–814. doi:10.2514/1.C031417.

[44] Suga, Y., and Yamazaki, W., "Aerodynamic Uncertainty Quantification of Supersonic Biplane Airfoil via Polynomial Chaos Approach," *AIAA SciTech Forum, 17th AIAA Non-Deterministic Approaches Conference*, Kissimmee, Florida, 2015. doi:10.2514/6.2015-1815.

[45] Lattarulo, V., Seshadri, P., and Parks, G. T., "Optimization of a supersonic airfoil using the multi-objective alliance algorithm," *Proceedings of the 15th annual conference on Genetic and evolutionary computation*, ACM, 2013, pp. 1333–1340. doi:10.1145/2463372.2463531.

[46] Tracy, R. R., "High efficiency, supersonic aircraft," , June 21 1994. US Patent 5,322,242.

[47] Gerhardt, H. A., Kerswell, J. F., Priestley, R. T., and Gibson, B. T., "Laminar supersonic transport aircraft," , December 1 1998. US Patent 5,842,666.

[48] Tracy, R. R., and Chase, J. D., "Lift and twist control using trailing edge control surfaces on supersonic laminar flow wings," , February 28 2006. US Patent 7,004,428.

[49] Kim, H.-J., Obayashi, S., and Nakahashi, K., "Flap-deflection optimization for transonic cruise performance improvement of supersonic transport wing," *Journal of aircraft*, Vol. 38, No. 4, 2001, pp. 709–717.

[50] Kenway, G. K. W., Kennedy, G. J., and Martins, J. R. R. A., "Scalable Parallel Approach for High-Fidelity Steady-State Aeroelastic Analysis and Derivative Computations," *AIAA Journal*, Vol. 52, No. 5, 2014, pp. 935–951. doi:10.2514/1.J052255.

[51] Lyu, Z., Kenway, G. K. W., and Martins, J. R. R. A., "RANS-based Aerodynamic Shape Optimization Investigations of the Common Research Model Wing," *Proceedings of the AIAA Science and Technology Forum and Exposition (SciTech)*, National Harbor, MD, 2014. doi:10.2514/6.2014-0567, aIAA 2014-0567.

[52] Bons, N. P., He, X., Mader, C. A., and Martins, J. R. R. A., "Multimodality in Aerodynamic Wing Design Optimization," *AIAA Journal*, Vol. 57, No. 3, 2019, pp. 1004–1018. doi:10.2514/1.J057294.

[53] Lyu, Z., Kenway, G. K. W., and Martins, J. R. R. A., "Aerodynamic Shape Optimization Investigations of the Common Research Model Wing Benchmark," *AIAA Journal*, Vol. 53, No. 4, 2015, pp. 968–985. doi:10.2514/1.J053318.

[54] Kenway, G. K. W., and Martins, J. R. R. A., "Multipoint Aerodynamic Shape Optimization Investigations of the Common Research Model Wing," *AIAA Journal*, Vol. 54, No. 1, 2016, pp. 113–128. doi:10.2514/1.J054154.

[55] Chen, S., Lyu, Z., Kenway, G. K. W., and Martins, J. R. R. A., "Aerodynamic Shape Optimization of the Common Research Model Wing-Body-Tail Configuration," *Journal of Aircraft*, Vol. 53, No. 1, 2016, pp. 276–293. doi:10.2514/1.C033328.

[56] Lyu, Z., and Martins, J. R. R. A., "Aerodynamic Design Optimization Studies of a Blended-Wing-Body Aircraft," *Journal of Aircraft*, Vol. 51, No. 5, 2014, pp. 1604–1617. doi:10.2514/1.C032491.

[57] Brooks, T. R., Martins, J. R. R. A., and Kennedy, G. J., "High-fidelity Aerostructural Optimization of Tow-steered Composite Wings," *Journal of Fluids and Structures*, Vol. 88, 2019, pp. 122–147. doi:10.1016/j.jfluidstructs.2019.04.005.

[58] Secco, N. R., and Martins, J. R. R. A., "RANS-based Aerodynamic Shape Optimization of a Strut-braced Wing with Overset Meshes," *Journal of Aircraft*, Vol. 56, No. 1, 2019, pp. 217–227. doi:10.2514/1.C034934.

[59] Sederberg, T. W., and Parry, S. R., "Free-form Deformation of Solid Geometric Models," *SIGGRAPH Comput. Graph.*, Vol. 20, No. 4, 1986, pp. 151–160. doi:10.1145/15886.15903.

[60] Kenway, G. K., Kennedy, G. J., and Martins, J. R. R. A., "A CAD-Free Approach to High-Fidelity Aerostructural Optimization," *Proceedings of the 13th AIAA/ISSMO Multidisciplinary Analysis Optimization Conference*, Fort Worth, TX, 2010. doi:10.2514/6.2010-9231.

[61] Luke, E., Collins, E., and Blades, E., "A Fast Mesh Deformation Method Using Explicit Interpolation," *Journal of Computational Physics*, Vol. 231, No. 2, 2012, pp. 586–601. doi:10.1016/j.jcp.2011.09.021.

[62] Kenway, G. K. W., and Martins, J. R. R. A., "Buffet Onset Constraint Formulation for Aerodynamic Shape Optimization," *AIAA Journal*, Vol. 55, No. 6, 2017, pp. 1930–1947. doi:10.2514/1.J055172.

[63] Mader, C. A., Kenway, G. K. W., Yildirim, A., and Martins, J. R. R. A., "ADflow—An open-source computational fluid dynamics solver for aerodynamic and multidisciplinary optimization," *Journal of Aerospace Information Systems*, 2020. doi:10.2514/1.I010796.

[64] Kenway, G. K. W., Mader, C. A., He, P., and Martins, J. R. R. A., "Effective Adjoint Approaches for Computational Fluid Dynamics," *Progress in Aerospace Sciences*, Vol. 110, 2019, p. 100542. doi:10.1016/j.paerosci.2019.05.002.

[65] Yildirim, A., Kenway, G. K. W., Mader, C. A., and Martins, J. R. R. A., "A Jacobian-free approximate Newton–Krylov startup strategy for RANS simulations," *Journal of Computational Physics*, Vol. 397, 2019, p. 108741. doi:10.1016/j.jcp.2019.06.018.

[66] Spalart, P., and Allmaras, S., "A One-Equation Turbulence Model for Aerodynamic Flows," *30th Aerospace Sciences Meeting and Exhibit*, 1992. doi:10.2514/6.1992-439.

[67] Gill, P. E., Murray, W., and Saunders, M. A., "SNOPT: An SQP algorithm for large-scale constrained optimization," *SIAM Journal of Optimization*, Vol. 12, No. 4, 2002, pp. 979–1006. doi:10.1137/S1052623499350013.

[68] Perez, R. E., Jansen, P. W., and Martins, J. R. R. A., "pyOpt: A Python-Based Object-Oriented Framework for Nonlinear Constrained Optimization," *Structural and Multidisciplinary Optimization*, Vol. 45, No. 1, 2012, pp. 101–118. doi: 10.1007/s00158-011-0666-3.

[69] Yu, Y., Lyu, Z., Xu, Z., and Martins, J. R. R. A., "On the Influence of Optimization Algorithm and Starting Design on Wing Aerodynamic Shape Optimization," *Aerospace Science and Technology*, Vol. 75, 2018, pp. 183–199. doi:10.1016/j.ast.2018.01.016.

[70] Chernukhin, O., and Zingg, D. W., "Multimodality and Global Optimization in Aerodynamic Design," *AIAA Journal*, Vol. 51, No. 6, 2013, pp. 1342–1354. doi: 10.2514/1.j051835.

[71] Martins, J. R. R. A., "Perspectives on Aerodynamic Design Optimization," *AIAA SciTech Forum*, AIAA, Orlando, FL, 2020. doi:10.2514/6.2020-0043.

[72] Mangano, M., and Martins, J. R. R. A., "Multipoint Aerodynamic Shape Optimization for Subsonic and Supersonic Regimes," *57th AIAA Aerospace Sciences Meeting, AIAA SciTech Forum, 2019*, San Diego, CA, 2019. doi:10.2514/6.2019-0696.

[73] Zhang, T.-t., Wang, Z.-g., Huang, W., and Yan, L., "A review of parametric approaches specific to aerodynamic design process," *Acta Astronautica*, 2018.

[74] Lindsey, W., Daley, B. N., and Humphreys, M. D., "The Flow and Force Characteristics of Supersonic Airfoils at High Subsonic Speeds, NASA Technical Note 1811," Tech. rep., NASA, 1947.

[75] Chan, W. M., and Steger, J. L., "Enhancements of a three-dimensional hyperbolic grid generation scheme," *Applied Mathematics and Computation*, Vol. 51, No. 2–3, 1992, pp. 181–205. doi:10.1016/0096-3003(92)90073-A.

[76] Norris, G., "Supersonic Evolution," *Aviation Week & Space Technology*, 2020, pp. 50–54.

[77] Bons, N. P., Martins, J. R. R. A., Mader, C. A., McMullen, M., and Suen, M., "High-fidelity Aerostructural Optimization Studies of the Aerion AS2 Supersonic Business Jet," *Proceedings of the AIAA Aviation Forum*, 2020. doi:10.2514/6.2020-3182.

[78] Burdette, D. A., and Martins, J. R. R. A., "Impact of Morphing Trailing Edge on Mission Performance for the Common Research Model," *Journal of Aircraft*, Vol. 56, No. 1, 2019, pp. 369–384. doi:10.2514/1.C034967.

[79] Mason, W. H., *Configuration aerodynamics*, Virginia Tech, 2006.

[80] Drela, M., *Frontiers of Computational Fluid Dynamics*, World Scientific, 1998, Chap. Pros and Cons of Airfoil Optimization, pp. 363–381. doi:10.1142/9789812815774_0019.

[81] Burdette, D. A., and Martins, J. R. R. A., "Design of a Transonic Wing with an Adaptive Morphing Trailing Edge via Aerostructural Optimization," *Aerospace Science and Technology*, Vol. 81, 2018, pp. 192–203. doi:10.1016/j.ast.2018.08.004.

[82] Palaniappan, K., and Jameson, A., "An analysis of bodies having minimum pressure drag in supersonic flow: Exploring the nonlinear domain," *Computational Fluid Dynamics 2004*, Springer, 2006, pp. 675–680. doi:10.1007/3-540-31801-1_98.